Thermodynamic topology of 4D dyonic AdS black holes in different ensembles

Naba Jyoti Gogoi* and Prabwal Phukon†

Department of Physics, Dibrugarh University, Dibrugarh 786004, Assam, India

(Received 3 May 2023; accepted 6 September 2023; published 25 September 2023)

We study the topology of the thermodynamic space of four dimensional dyonic anti–de Sitter (AdS) black hole in three different ensembles: canonical, mixed, and grand canonical ensemble. While canonical ensemble refers to the ensemble with fixed electric and magnetic charges, mixed ensemble is an ensemble where we fix magnetic charge and electric potential. In the grand canonical ensemble, potentials corresponding to both electric and magnetic charges are kept fixed. In each of these ensembles, we first compute the topological charges associated with critical points. We find that while in both canonical and mixed ensembles, there exists one conventional critical point with topological charge -1, in the grand canonical ensemble, we find no critical point. Then, we consider the dyonic AdS black hole as topological defects in thermodynamic space and study its local and global topology by computing the winding numbers at the defects. We observe that while the topologies of the black hole in canonical and mixed ensembles are identical with total topological charge equaling 1, in the grand canonical ensemble, depending on the values of potentials, the total topological charge is either equal to 0 or 1. In canonical and mixed ensembles, either one generation and one annihilation points or no generation/annihilation points are found. In the grand canonical ensemble, depending on the values of potentials, we find either one generation point or no generation/annihilation point. Thus, we infer that the topological class of 4D dyonic AdS black hole is ensemble dependent.

DOI: 10.1103/PhysRevD.108.066016

I. INTRODUCTION

Thermodynamic phase behavior of black holes has been studied extensively since the early days of black hole thermodynamics [1–14]. In recent years, a lot of focus has been attributed to the study of criticality in AdS black holes in extended thermodynamic space [15–26], where the cosmological constant Λ is considered as thermodynamic pressure P [27–30].

$$P = -\frac{\Lambda}{8\pi G}, \tag{1}$$

where, G is Newton's gravitational constant. Accordingly, a thermodynamic volume V is defined conjugate to thermodynamic pressure P and the first law of black hole thermodynamics takes the revised form:

$$dM = TdS + VdP + \sum_i Y_i dx^i, \tag{2}$$

where, T is the temperature, S is the entropy, and $Y_i dx^i$ is the ith chemical potential term.

A recent addition to the study of criticality in black holes is the idea of thermodynamic topology. Initiated in [31], in this novel approach, Duan's topological current ϕ-mapping theory [32] is invoked in the thermodynamic space of a black hole to study its criticality. Consequently, the critical points in the thermodynamic space are characterized with distinct topological charges and based on those charges, are classified into conventional and novel critical points. The key steps involved are summarized below:

The temperature, T, of a black hole is expressed as a function of pressure P, entropy S and other thermodynamic parameters.

$$T = T(S, P, x^i), \tag{3}$$

where x^i denotes other thermodynamic parameters. The critical points can be calculated by the conditions $(\partial_S T)_{P,x^i} = 0$ and $(\partial_{S,S} T)_{P,x^i} = 0$. One can eliminate a thermodynamic parameter from T using these conditions and construct a Duan's potential Φ with a factor $1/\sin\theta$ [31]. Hence, by eliminating P using $(\partial_S T)_{P,x^i} = 0$, the

*gogoin799@gmail.com
†prabwal@dibru.ac.in

scalar thermodynamic function or the Duan's potential Φ is obtained as

$$\Phi = \frac{1}{\sin\theta} T(S, x^i). \tag{4}$$

Here, θ is an additional parameter and the inverse of sin of this parameter eases the calculation in the following ways: first, it sets a boundary for the vector field ϕ which is between $\theta = 0$ and $\theta = \pi$. Second, the zero point of ϕ is always located at $\theta = \pi/2$. A two dimensional vector $\phi = (\phi^\theta, \phi^\theta)$ is defined following the framework of Duan's ϕ-mapping theory [32,33] as

$$\phi^S = (\partial_S \Phi)_{\theta, x^i}, \qquad \phi^\theta = (\partial_\theta \Phi)_{S, x^i}. \tag{5}$$

The presence of θ in the vector field ϕ ensures that the zero point of the vector field ϕ is always at $\theta = \pi/2$. The critical points can be calculated using this criteria. Also the topological current, j^μ, is conserved, i.e., $\phi^a(x^i) = 0$. This construction ensures the existence of topological charge which for a given parameter region Σ is equal to

$$Q = \int_\Sigma j^0 d^2x = \sum_{i=1}^{N} \beta_i n_i = \sum_{i=1}^{N} w_i. \tag{6}$$

Here, w_i, j^0, and β_i are the winding number of ith zero points of ϕ, the density of the topological current and the Hopf index respectively. Critical points with topological charges -1 and $+1$ are referred as conventional critical point and novel critical point respectively. The total topological charge of a black hole is computed as the sum of individual charges associated with each critical point. The formalism can be followed with different thermodynamic parameters other than S. For example, the formalism is same for horizon radius r_+ as S can be reduced to r_+. Following the work in [31], analysis of thermodynamic topology has been extended to a number of black holes [34–40].

An alternative way to apply topology in black hole thermodynamics has also been proposed in [41]. In this method, black hole solutions are regarded as defects in thermodynamic parameter spaces. These defects are then studied in terms of their winding numbers. The sign of the winding number of a defect has been linked to the thermodynamic stability of the corresponding black hole solution. The sum of the winding numbers is, now, termed as topological number based on which different black hole solutions are categorized. The analysis begins with the introduction of a generalized free energy F defined as follows:

$$\mathcal{F} = E - \frac{S}{\tau}, \tag{7}$$

where E and S are the energy, entropy. τ is a quantity which has the dimension of time. A vector field ϕ is defined from F in the following way:

$$\phi = \left(\frac{\partial \mathcal{F}}{\partial r_+}, -\cot\Theta \csc\Theta \right). \tag{8}$$

The zero point of the vector ϕ is at $\Theta = \pi/2$. The unit vector is defined as

$$n^a = \frac{\phi^a}{||\phi||} \quad (a = 1,2) \quad \text{and} \quad \phi^1 = \phi^{r_+}, \qquad \phi^2 = \phi^\Theta. \tag{9}$$

Corresponding to a given value of τ, the zero points of n^1 are computed. The winding numbers of each of these zero points are calculated. The topological number of a black hole is obtained by summing over the individual winding numbers of all the black hole branches. Following [41], study of black holes as topological defects has been extended to a number of black holes in [42–52].

Motivated by all the above mentioned works, in this paper, we extend the study of thermodynamic topology to 4d dyonic AdS black hole in different ensembles. Our primary focus is to understand the ensemble dependent nature of thermodynamic topology. For this, we carry out our analysis in three different ensembles: (1) canonical ensemble where both the electric and the magnetic charges are kept fixed, (2) mixed ensemble where electric potential and magnetic charge are kept fixed, and (3) grand canonical ensemble where both electric and magnetic potentials are kept fixed. To begin with, in each of these ensembles, we figure out the critical points and compute their topological charges. Based on the sign of those charges, we classify them as conventional and novel critical points. Then we consider the black hole as a topological defect in each of these ensembles and find out its topological number, generation and annihilation points in the thermodynamic space.

This paper is organized as follows. In Sec. II, we begin with 4d dyonic AdS black hole in canonical ensemble and study its thermodynamic topology. This is followed by similar studies in mixed ensemble in Sec. III and grand canonical ensemble in Sec. IV. We conclude with our findings in Sec. V.

II. 4D DYONIC AdS BLACK HOLE IN CANONICAL ENSEMBLE

The four dimensional, asymptotically anti-de Sitter, dyonic black holes solution has its origin in maximal gauged supergravity. Such a black hole carries both electric and magnetic charges. The dyonic black hole solution can be obtained by the reduction of five dimensional Kaluza-Klein theory and it has some very interesting properties [53–58]. A simpler solution of dyonic AdS black hole can be obtained by varying the Reissner-Nordström action with

a cosmological constant [59]. The four dimensional, asymptotically anti–de Sitter, dyonic black hole metric is given by:

$$ds^2 = -f(r)dt^2 + \frac{1}{f(r)}dr^2 + r^2 d\theta^2 + r^2 \sin^2\theta d\phi^2, \quad (10)$$

where,

$$f(r) = \frac{q_e^2 + q_m^2}{r^2} + \frac{r^2}{l^2} - \frac{2M}{r} + 1, \quad (11)$$

Here, q_e, q_m, M, and l are electric charge, magnetic charge, mass of the black hole and the AdS radius respectively. Thermodynamic pressure, P, is related to the AdS radius as

$$P = \frac{3}{8\pi l^2}. \quad (12)$$

The mass, M and the entropy, S of the black hole are given by (in the following expressions, r_+ denotes the horizon radius)

$$M = \frac{l^2 q_e^2 + l^2 q_m^2 + l^2 r_+^2 + r_+^4}{2l^2 r_+} = \frac{3q_e^2 + 3q_m^2 + 8\pi P r_+^4 + 3r_+^2}{6r_+} \quad (13)$$

$$S = \pi r_+^2. \quad (14)$$

A. Topology of 4d dyonic AdS black hole thermodynamics in canonical ensemble

To study the topology of dyonic AdS black hole thermodynamics, we write the temperature as a function of pressure, horizon radius, electric, and magnetic charges.

$$T = \frac{\partial_{r_+} M}{\partial_{r_+} S} = \frac{8\pi P r_+^4 + r_+^2 - q_e^2 - q_m^2}{4\pi r_+^3}. \quad (15)$$

Use of the condition $\left(\frac{\partial_{r_+} T}{\partial_{r_+} S}\right)_{q_e, q_m, P} = 0$ leads us to an expression for pressure, P.

$$P = \frac{r_+^2 - 3(q_e^2 + q_m^2)}{8\pi r_+^4}, \quad (16)$$

Plugging P in (15), we get rid of the pressure term and the temperature, T takes the following form:

$$T(q_e, q_m, r_+) = \frac{r_+^2 - 2(q_e^2 + q_m^2)}{2\pi r_+^3}. \quad (17)$$

A thermodynamic function Φ is defined as,

$$\Phi = \frac{1}{\sin\theta} T(q_e, q_m, r_+) = \frac{\csc\theta\{r_+^2 - 2(q_e^2 + q_m^2)\}}{2\pi r_+^3}, \quad (18)$$

The vector components of the vector field $\phi = (\phi^{r_+}, \phi^\theta)$ are

$$\phi^{r_+} = \left(\frac{\partial \Phi}{\partial r_+}\right)_{q_e, q_m, \theta} = -\frac{\csc\theta\{r_+^2 - 6(q_e^2 + q_m^2)\}}{2\pi r_+^4}, \quad (19)$$

and

$$\phi^\theta = \left(\frac{\partial \Phi}{\partial \theta}\right)_{q_e, q_m, r_+} = -\frac{\cot\theta \csc\theta\{r_+^2 - 2(q_e^2 + q_m^2)\}}{2\pi r_+^3} \quad (20)$$

The normalized vector components are

$$\frac{\phi^{r_+}}{\|\phi\|} = \frac{6(q_e^2 + q_m^2) - r_+^2}{\sqrt{r_+^2 \cot^2(\theta)(r_+^2 - 2(q_e^2 + q_m^2))^2 + (r_+^2 - 6(q_e^2 + q_m^2))^2}}, \quad (21)$$

and

$$\frac{\phi^\theta}{\|\phi\|} = -\frac{r_+ \cot\theta\{r_+^2 - 2(q_e^2 + q_m^2)\}}{\sqrt{r_+^2 \cot^2\theta\{r_+^2 - 2(q_e^2 + q_m^2)\}^2 + \{r_+^2 - 6(q_e^2 + q_m^2)\}^2}} \quad (22)$$

The normalized vector $n = \left(\frac{\phi^{r_+}}{\|\phi\|}, \frac{\phi^\theta}{\|\phi\|}\right)$ has been plotted in Fig. 1. This figure shows the vector plot of n in a r_+ vs θ plane for dyonic AdS black hole. For this plot, we have fixed $q_e = q_m = 1$. The black dot represents the critical point (CP_1). To calculate the critical point we set $\theta = \pi/2$ in (21) and equate this to zero. The critical point is located at $(r_+, \theta) = (\sqrt{6(q_e^2 + q_m^2)}, \pi/2)$ or at $(r_+, \theta) = (2\sqrt{3}, \pi/2)$ for $q_e = q_m = 1$.

For the calculation of the topological charge of the critical point, a contour C parametrized by $\vartheta \in (0, 2\pi)$ is defined [31] as follows:

$$\begin{cases} r_+ = a\cos\vartheta + r_0, \\ \theta = b\sin\vartheta + \frac{\pi}{2}. \end{cases} \quad (23)$$

We construct two contours C_1 and C_2 where the first contour encloses the critical point CP_1 and the second

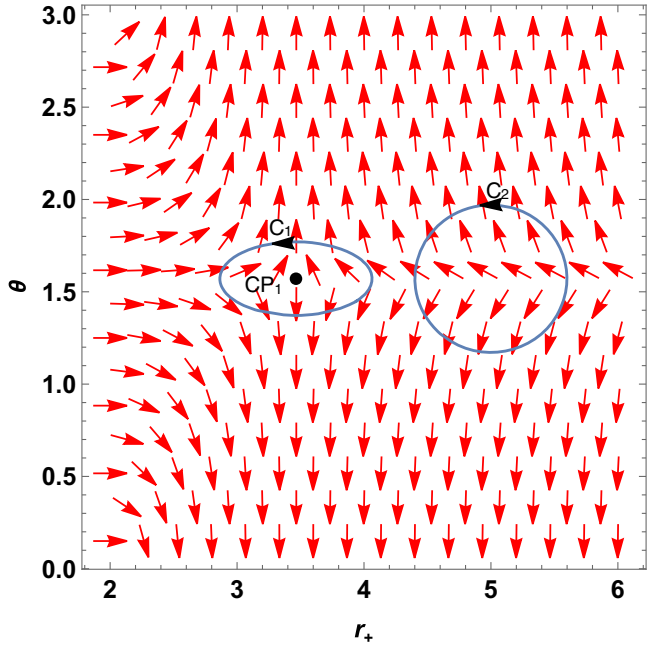

FIG. 1. Plot of the normalized vector field n in r_+ vs θ plane for dyonic AdS black hole in canonical ensemble. The black dot represents the critical point.

contour is outside the critical point. For these contours we choose $(a, b, r_0) = (0.6, 0.2, 2\sqrt{3})$ and (0.6, 0.4, 5).

The deflection of the vector field n along the contour C is,

$$\Omega(\vartheta) = \int_0^{\vartheta} \epsilon_{ab} n^a \partial_\vartheta n^b d\vartheta. \tag{24}$$

The topological charge is, then, equal to, $Q = \frac{1}{2\pi}\Omega(2\pi)$. For the critical point CP_1 enclosed by the contour C_1, the topological charge has been found to be, $Q_{CP_1} = -1$. This is a conventional critical point. Since the contour C_2 does not enclose any critical point, it corresponds to zero topological charge. Thus, the total topological charge is, $Q = -1$. The behavior of Ω is shown in Fig. 2. The red curve corresponds C_1 and the blue curve corresponds to C_2. The function $\Omega(\vartheta)$ for C_1 decreases non-linearly and reaches -2π at $\vartheta = 2\pi$. On the other hand, $\Omega(\vartheta)$ reaches zero at $\vartheta = 2\pi$ for C_2.

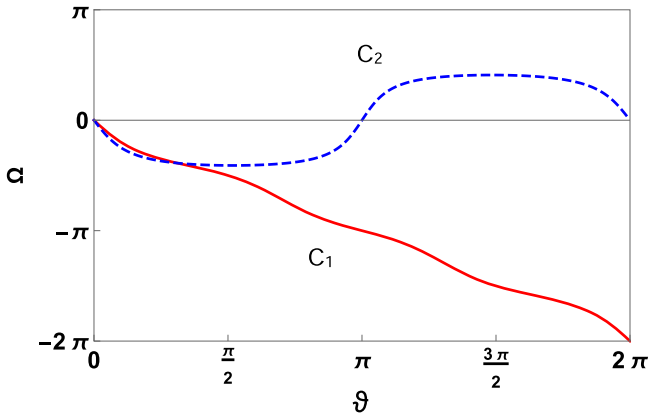

FIG. 2. Ω vs ϑ plot for the contour $C1$ and C_2.

4d dyonic AdS black hole in canonical ensemble has the following equation of state:

$$T = \frac{8\pi P r_+^4 + r_+^2 - q_e^2 - q_m^2}{4\pi r_+^3}, \tag{25}$$

The corresponding critical points are given by,

$$T_c = \frac{1}{3\sqrt{6}\pi\sqrt{q_e^2 + q_m^2}}, \qquad P_c = \frac{1}{96\pi q_e^2 + 96\pi q_m^2}$$

$$\text{and} \quad r_c = \sqrt{6(q_e^2 + q_m^2)}. \tag{26}$$

It can be clearly seen that the critical radius in (26) exactly matches the critical point obtained from thermodynamic topology, $(r_+, \theta) = (\sqrt{6(q_e^2 + q_m^2)}, \pi/2)$. As mentioned above this is a conventional critical point with topological charge −1. To see the nature of the critical point we plot the phase structure (isobaric curves) around it in Fig. 3. The location of the critical point in the isobaric curve is shown as a black dot. The red curve is the isobaric curve for $P = P_c$. The green curves above and below the red curve are respectively for $P > P_c$ and $P < P_c$. The blue dashed curvet describes the extremal points and is plotted using (17). From Fig. 3, it is observed that for $P < P_c$, the small and large black hole phases are separated by the unstable region (the negative slope region of the isobaric curves or the region enclosed by the two extremal points corresponding to each isobaric curve). Different phases of the dyonic AdS black hole in canonical ensemble disappear at the critical point. Hence, the critical point CP_1 can be thought of as a phase annihilation point.

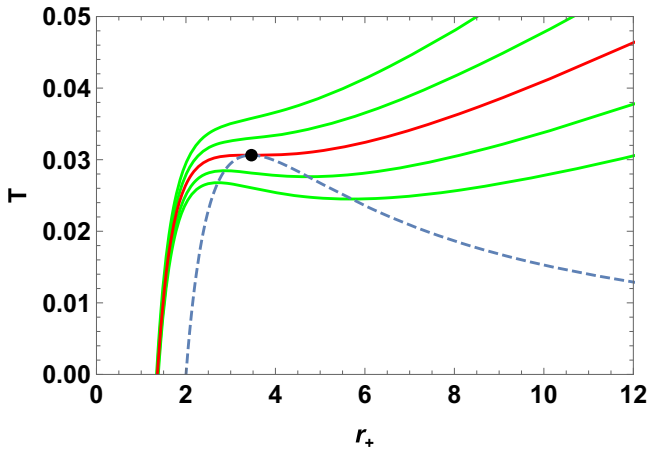

FIG. 3. Isobaric curves (red and green) of dyonic AdS black hole in canonical ensemble. Black dot represents the critical point.

B. Dyonic AdS black hole solution as topological thermodynamic defects in canonical ensemble

Now, we proceed to study the dyonic AdS black hole solution in canonical ensemble as topological thermodynamic defects. Using the mass and entropy of the black hole from (13) and (14) in (7), the generalized free energy is found to be,

$$\mathcal{F} = \frac{3q_e^2 + 3q_m^2 + 8\pi P r_+^4 + 3r_+^2}{6r_+} - \frac{\pi r_+^2}{\tau}. \tag{27}$$

The vector field components of the vector given by (8) are

$$\phi^{r_+} = \frac{1}{2} - \frac{q_e^2 + q_m^2}{2r_+^2} + 4\pi P r_+^2 - \frac{2\pi r_+}{\tau}, \tag{28}$$

and

$$\phi^{\Theta} = -\cot\Theta \csc\Theta. \tag{29}$$

The corresponding unit vectors are

$$n^1 = \frac{4\pi r_+^3(2Pr_+\tau - 1) - \tau(q_e^2 + q_m^2 - r_+^2)}{r_+^2\tau\sqrt{\frac{\{\tau(q_e^2+q_m^2-r_+^2)+4\pi r_+^3(1-2Pr_+\tau)\}^2}{r_+^4\tau^2} + 4\cot^2\Theta\csc^2\Theta}}, \tag{30}$$

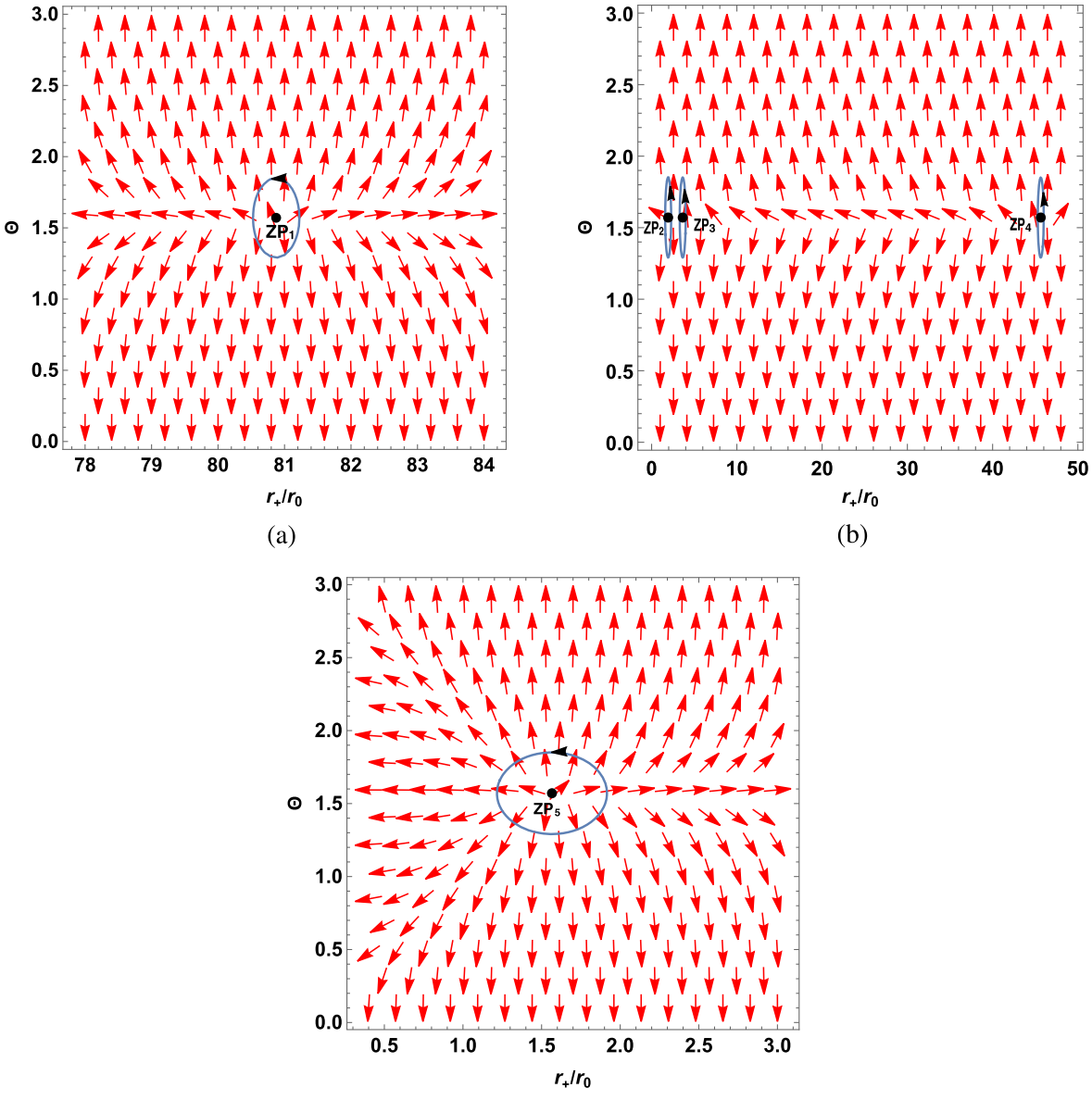

FIG. 4. Unit vector $n = (n^1, n^2)$ shown in Θ vs r_+/r_0 plane for $Pr_0^2 = 0.0002$ (below critical pressure P_c). The black dots represent the zero points. (a) Unit vector n in Θ vs r_+/r_0 plane for $\tau/r_0 \times = 30$. (b) Unit vector n in Θ vs r_+/r_0 plane for $\tau/r_0 \times = 50$. The zero points are ZP_2, ZP_3, and ZP_4 from left to right. (c) Unit vector Unit vector n in Θ vs r_+/r_0 plane for $\tau/r_0 \times = 100$.

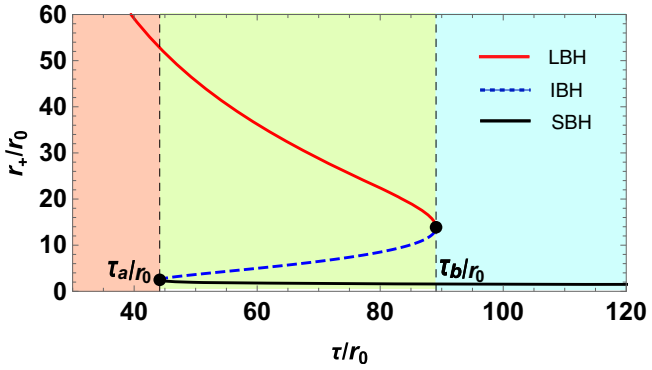

FIG. 5. The zero points of ϕ^{r_+} in τ/r_0 vs r_+/r_0 plane for dyonic AdS black hole in canonical ensemble for pressure less than the critical pressure P_c.

and

$$n^2 = -\frac{\cot\Theta\csc\Theta}{\sqrt{\frac{\{\tau(q_e^2+q_m^2-r_+^2)+4\pi r_+^3(1-2Pr_+\tau)\}^2}{4r_+^4\tau^2}+\cot^2\Theta\csc^2\Theta}}. \quad (31)$$

These unit vectors are plotted and used to locate the zero points by setting $\Theta = \pi/2$ in n^1 [see (30)] and equating it to zero. For example, setting $q_e/r_0 = 1$, $q_m/r_0 = 1$, $Pr_0^2 = 0.0002$, and $\tau/r_0 = 30$, we can find one zero point (ZP_1) located at $(r_+/r_0, \Theta) = (80.8742, \pi/2)$. Here, r_0 is an arbitrary length scale which is determined by the size of a cavity that surrounds the black hole. The value of pressure is taken below the critical pressure P_c. The representation of the unit vectors along with the zero point is shown in Fig. 4(a). The winding number or the topological charge corresponding to this zero point is computed following the prescription stated in the previous section and found to be $w = +1$. Similarly, keeping the same charge and pressure configuration, corresponding to $\tau/r_0 = 50$, we find three zero points ZP_2, ZP_3, and ZP_4 with winding numbers $+1$, -1, and $+1$ respectively. These are shown in Fig. 4(b). For $\tau/r_0 = 100$, a solitary zero point ZP_5 with winding number $+1$ is observed [Fig. 4(c)].

An analytic expression for τ corresponding to zero points can be obtained by setting $\phi^{r_+} = 0$.

$$\tau = \frac{4\pi r_+^3}{8\pi P r_+^4 + r_+^2 - q_e^2 - q_m^2}. \quad (32)$$

A plot of r_+ vs τ obtained above is shown in Fig. 5. The points on this curve are the zero points of ϕ^{r_+}. Here, we have fixed $q_e/r_0 = 1$, $q_m/r_0 = 1$, and $Pr_0^2 = 0.0002$ (below the critical pressure P_c).

In Fig. 5, three different black hole branches are clearly visible. The branch $\tau < \tau_b$ corresponds to the large black hole region. The winding number for any zero point on this branch is found to be $w = +1$. Similarly, winding number $w = +1$ is also observed for any zero point on the branch $\tau > \tau_a$ which corresponds to the small black hole region. The branch $\tau_a < \tau < \tau_b$ represents the intermediate black hole region and winding number for any zero point on this branch is equal to $w = -1$. The topological number is, hence, $W = +1 - 1 + 1 = +1$. We explicitly computed the specific heats at the three branches and found that the branches with winding number $+1$ have positive specific heat (thermodynamically stable) and the branch with winding number -1 has negative specific heat (thermodynamically unstable).

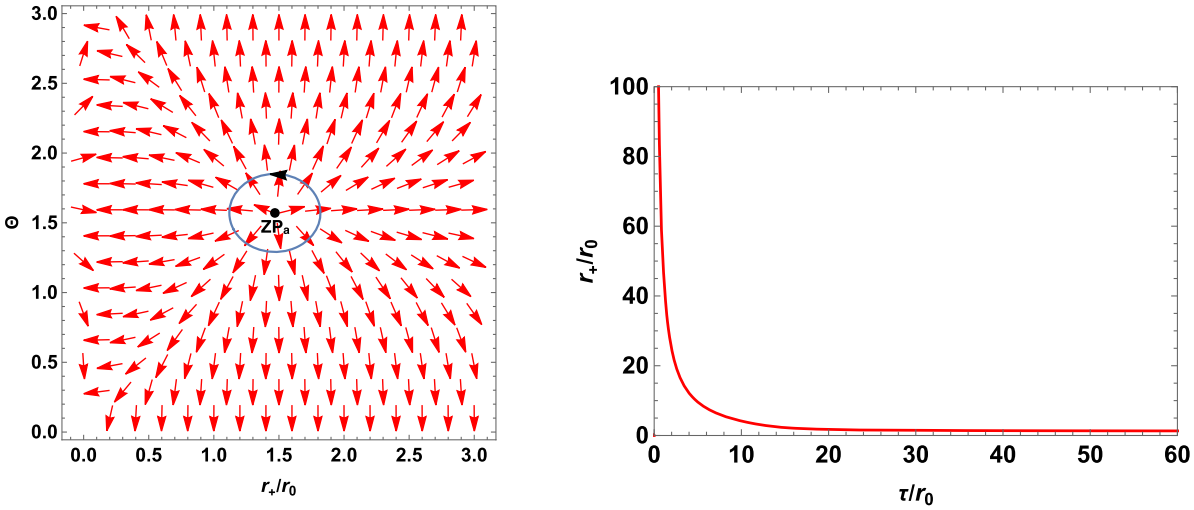

(a) (b)

FIG. 6. Plot of unit vector $n = (n^1, n^2)$ and zero point of ϕ^{r_+} for pressure $Pr_0^2 = 0.01$ (above the critical pressure P_c). (a) Unit vector $n = (n^1, n^2)$ shown in Θ vs r_+/r_0 plane for $Pr_0^2 = 0.01$. The black dot represents zero point. (b) The zero points of ϕ^{r_+} in τ/r_0 vs r_+/r_0 plane for dyonic AdS black hole in mixed ensemble for pressure greater than the critical pressure P_c.

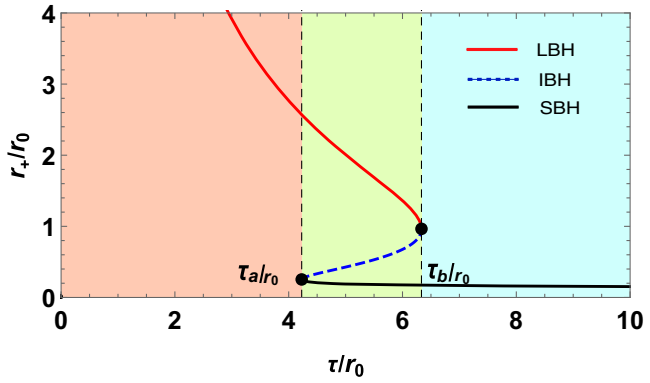

FIG. 7. The zero points of ϕ^{r_+} in τ/r_0 vs r_+/r_0 plane for dyonic AdS black hole in canonical ensemble for $q_e/r_0 = 0.1$, $q_m/r_0 = 0.1$, and $Pr_0^2 = 0.04$.

Finally, we find the generation/annihilation points by using the condition $\partial_{r_+}\mathcal{F} = \partial_{r_+,r_+}\mathcal{F} = 0$. For $q_e/r_0 = 1$, $q_m/r_0 = 1$, $Pr_0^2 = 0.0002$, we get the generation and annihilation points at $\tau/r_0 = \tau_a/r_0 = 44.1585$ and $\tau/r_0 = \tau_b/r_0 = 89.0811$ respectively which are shown as black dots in Fig. 5.

For a value of pressure, $Pr_0^2 = 0.01$, which is above the critical pressure P_c, and $q_e/r_0 = q_m/r_0 = 1$, the plot of r_+ vs τ is shown in Fig. 6(b). In this case, the plot exhibits only one branch corresponding to stable black hole region with positive specific heat. The winding numbers of zero points on this branch is computed to be $w = +1$. The topological number is, hence, $W = +1$. Notably, we do not find any generation/annihilation point in this case. The zero point for $\tau/r_0 = 30$, $q_m/r_0 = q_e/r_0 = 1$, $Pr_0^2 = 0.01$ is shown in Fig. 6(a). What we have seen is that the topological number of $4d$ dyonic AdS black hole in canonical ensemble is not altered by a variation in pressure.

We repeated our analysis by changing the values of q_e and q_m. We found that the topological number was always equal to $(W = +1)$ for all the charge configurations. As an example, the r_+ vs τ curve for $q_e/r_0 = 0.1$, $q_m/r_0 = 0.1$, and $Pr_0^2 = 0.04$ is shown in Fig. 7. The topological number of $4d$ dyonic AdS black hole in canonical ensemble is not influenced by a variation in charge configuration.

III. DYONIC AdS BLACK HOLE IN MIXED ENSEMBLE

In mixed ensemble, the electric potential ϕ_e and the magnetic charge q_m are kept constant. The electric potential ϕ_e is defined as

$$\phi_e = \frac{q_e}{r_+}, \tag{33}$$

The mass and temperature, are, then modified as

$$M = \frac{3r_+^2\phi_e^2 + 3q_m^2 + 8\pi P r_+^4 + 3r_+^2}{6r_+}, \tag{34}$$

and

$$T = \frac{8\pi P r_+^4 + r_+^2 - r_+^2\phi_e^2 - q_m^2}{4\pi r_+^3}. \tag{35}$$

A. Topology of dyonic AdS black hole in mixed ensemble

In this section, we study the thermodynamic topology of $4d$ dyonic AdS black hole in mixed ensemble. We begin by eliminating pressure from (35) which is then simplified to

$$T(\phi_e, q_m, r_+) = -\frac{r_+^2(\phi_e^2 - 1) + 2q_m^2}{2\pi r_+^3}, \tag{36}$$

and the thermodynamic function Φ becomes

$$\Phi = \frac{1}{\sin\theta}T(\phi_e, q_m, r_+) = -\frac{\csc\theta\{r_+^2(\phi_e^2 - 1) + 2q_m^2\}}{2\pi r_+^3} \tag{37}$$

The vector components of $\phi = (\phi^{r_+}, \phi^\theta)$ are given by,

$$\phi^{r_+} = \frac{\csc\theta\{r_+^2(\phi_e^2 - 1) + 6q_m^2\}}{2\pi r_+^4}, \tag{38}$$

and

$$\phi^\theta = \frac{\cot\theta\csc\theta\{r_+^2(\phi_e^2 - 1) + 2q_m^2\}}{2\pi r_+^3} \tag{39}$$

The vector ϕ is normalized and the components are

$$\frac{\phi^{r_+}}{\|\phi\|} = \frac{r_+^2(\phi_e^2 - 1) + 6q_m^2}{\sqrt{r_+^2\cot^2\theta\{r_+^2(\phi_e^2 - 1) + 2q_m^2\}^2 + \{r_+^2(\phi_e^2 - 1) + 6q_m^2\}^2}}, \tag{40}$$

and

$$\frac{\phi^\theta}{\|\phi\|} = \frac{r_+\cot\theta(r_+^2(\phi_e^2 - 1) + 2q_m^2)}{\sqrt{r_+^2\cot^2\theta\{r_+^2(\phi_e^2 - 1) + 2q_m^2\}^2 + \{r_+^2(\phi_e^2 - 1) + 6q_m^2\}^2}}. \tag{41}$$

Now, we plot the normalized vector $n = \left(\frac{\phi^{r_+}}{\|\phi\|}, \frac{\phi^\theta}{\|\phi\|}\right)$ in r_+ vs θ plane by fixing $q_m = 1$ and $\phi_e = 1/2$ (see Fig. 8). Here,

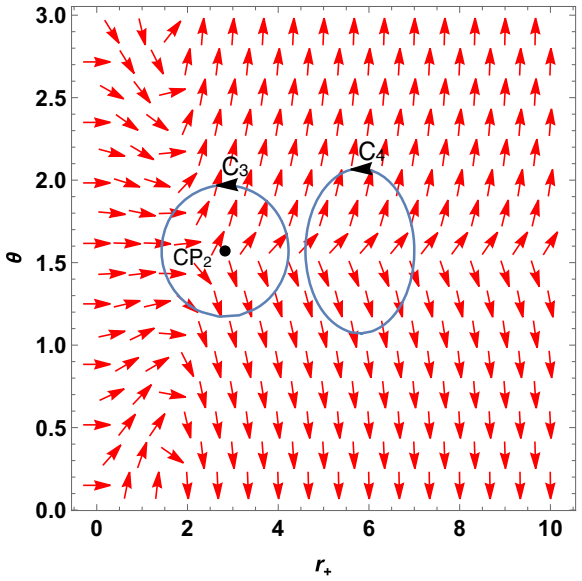

FIG. 8. Plot of the normalized vector field n in r_+ vs θ plane for dyonic AdS black hole in mixed ensemble. The black dot represents the critical point.

we find a single critical point CP_2 at $(r_+, \theta) = (\sqrt{6}q_m/\sqrt{1-\phi_e^2}, \pi/2)$ represented by the black dot.

We draw two contours C_3 and C_4 for $(a, b, r_0) = (1.4, 0.4, 2\sqrt{2})$ and $(1.2, 0.5, 5.8)$. The contour C_3 encloses the critical point CP_2 whereas C_4 does not enclose any critical point. The topological charge corresponding to the contour C_3 is -1 which implies that it is a conventional critical point. The contour C_4 does not enclose any critical point and hence the topological charge is 0. The total topological charge is -1. The deflection along the contour C_3 and C_4 is shown in Fig. 9. The equation of state for the black hole in mixed ensemble is given by,

$$T = \frac{8\pi P r_+^4 + r_+^2 - r_+^2\phi_e^2 - q_m^2}{4\pi r_+^3}. \tag{42}$$

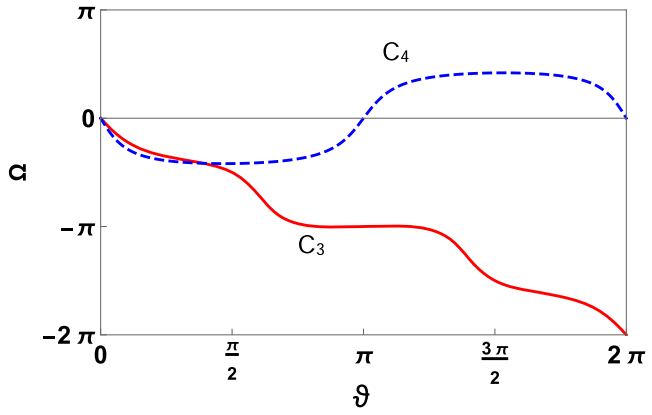

FIG. 9. Ω vs ϑ plot for the contour $C3$ and C_4.

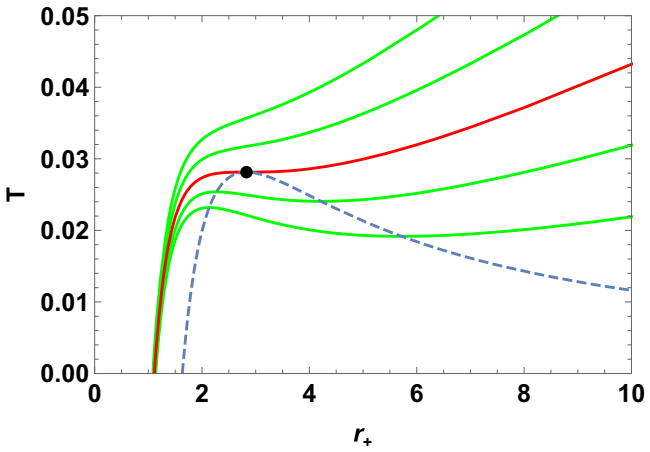

FIG. 10. Isobaric curves (red and green) of dyonic AdS black hole in mixed ensemble. Red curve is the isobaric curve for $P = P_c$. The isobaric curves above and below the red curve is for $P > P_c$ and $P < P_c$ respectively. Black dot represents the critical point.

The critical values are

$$T_c = \frac{(1-\phi_e^2)^{3/2}}{3\sqrt{6}\pi q_m}, \qquad P_c = \frac{(\phi_e^2-1)^2}{96\pi q_m^2} \quad \text{and}$$
$$r_c = \frac{\sqrt{6}q_m}{\sqrt{1-\phi_e^2}}. \tag{43}$$

In this ensemble also, we see that the critical radius given in (43) is exactly the same as the conventional critical point which is $(r_+, \theta) = (\sqrt{6}q_m/\sqrt{1-\phi_e^2}, \pi/2)$. We plot the T vs r_+ isobaric curve around the critical point in Fig. 10. This figure shows that the critical point (black dot) is on the isobaric curve for $P = P_c$ (red curve). The blue curve gives the extremal points of the isobaric curves and is plotted using (36). Similar to the canonical ensemble case, the number of phases clearly decreases with the increase of pressure P and disappears at the critical point CP_3. This implies that the critical point CP_3 is a phase annihilation point.

B. Dyonic AdS black hole solution as topological thermodynamic defects in mixed ensemble

We now study the dyonic AdS black hole in mixed ensemble as a topological defect. As usual, we start with the generalized free energy potential

$$\mathcal{F} = E - \frac{S}{\tau} - q_e\phi_e. \tag{44}$$

In this ensemble

$$E = \frac{3r_+^2\phi_e^2 + 3q_m^2 + 8\pi P r_+^4 + 3r_+^2}{6r_+},$$
$$S = \pi r_+^2 \quad \text{and} \quad q_e = r_+\phi_e \tag{45}$$

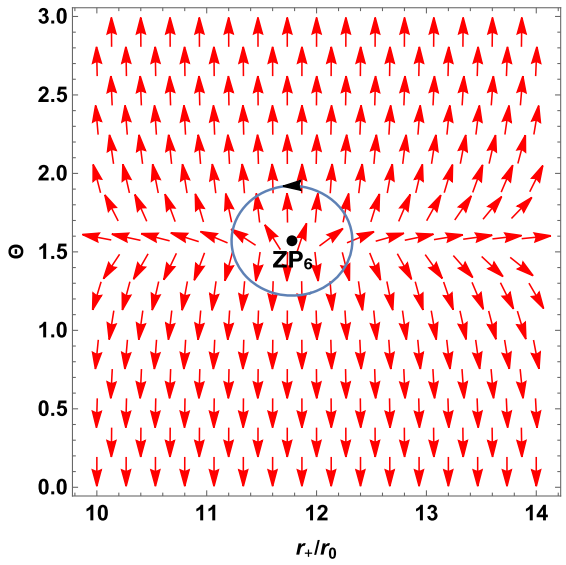

(a) Unit vector n in Θ vs r_+/r_0 plane for $\tau/r_0 = 35$

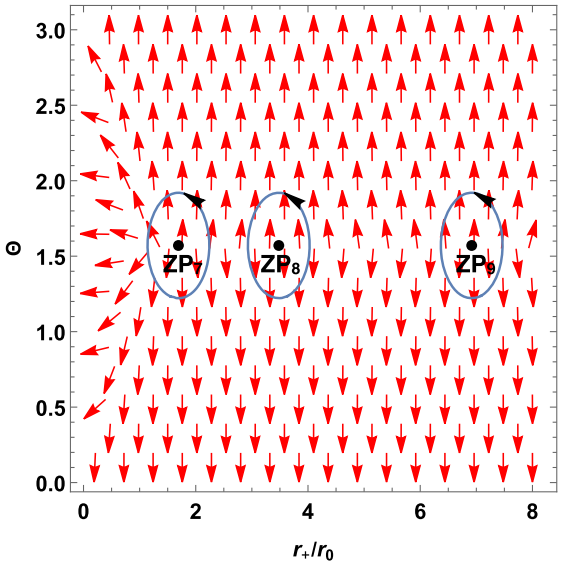

(b) Unit vector n in Θ vs r_+/r_0 plane for $\tau/r_0 = 45$.

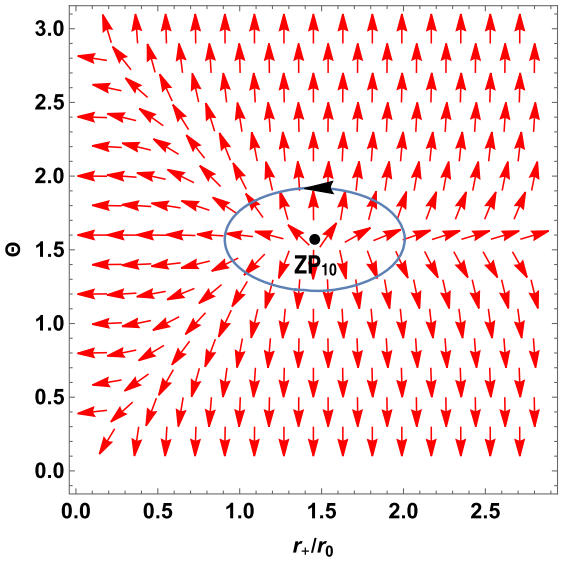

(c) Unit vector n in Θ vs r_+/r_0 plane for $\tau/r_0 = 55$

FIG. 11. Unit vector $n = (n^1, n^2)$ shown in Θ vs r_+/r_0 plane for $Pr_0^2 = 0.001$ (pressure point below the critical pressure P_c). The black dots represent the zero points.

Hence, (44) gives

$$\mathcal{F} = \frac{3r_+^2\phi_e^2 + 3q_m^2 + 8\pi P r_+^4 + 3r_+^2}{6r_+} - r_+\phi_e^2 - \frac{\pi r_+^2}{\tau}. \quad (46)$$

From (8), the vector components can easily be worked out resulting

$$\phi^{r_+} = \frac{6r_+\phi_e^2 + 32\pi P r_+^3 + 6r_+}{6r_+} - \frac{3r_+^2\phi_e^2 + 3q_m^2 + 8\pi P r_+^4 + 3r_+^2}{6r_+^2} - \phi_e^2 - \frac{2\pi r_+}{\tau}, \quad (47)$$

and

$$\phi^{\Theta} = -\cot\Theta \csc\Theta. \quad (48)$$

We plot the normalized vector and figure out the zero points. The corresponding winding numbers are also calculated. For different values of τ/r_0 the zero points are shown in Fig. 11. Here, we have set $\phi_e = 1/2$, $q_m/r_0 = 1$, $Pr_0^2 = 0.001$ (pressure value below the critical pressure P_c). While for $\tau/r_0 = 35$, we find one zero point ZP_6 with winding number $+1$, for $\tau/r_0 = 45$, we locate three zero points ZP_7, ZP_8, and ZP_9 with winding numbers

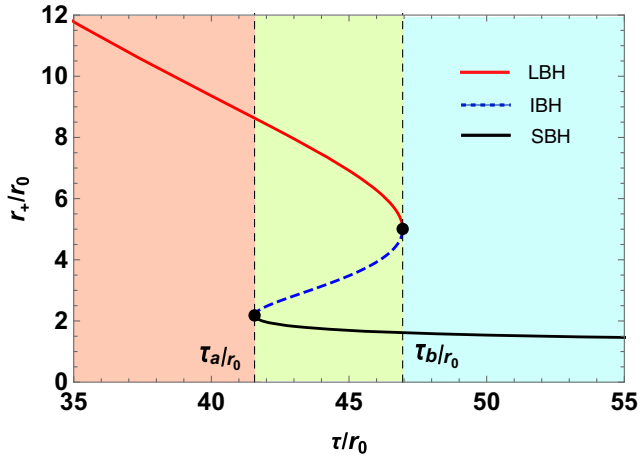

FIG. 12. The zero points of ϕ^{r_+} in τ/r_0 vs r_+/r_0 plane for dyonic AdS black hole in mixed ensemble below the critical pressure P_c.

$+1, -1$, and $+1$ respectively. For $\tau/r_0 = 55$, we again encounter one zero point $ZP_1 0$ with winding number $+1$.

The zero points of the component $\phi^{r_+} = 0$ are given by the equation

$$\tau = \frac{4\pi r_+^3}{8\pi P r_+^4 + r_+^2 - r_+^2\phi_e^2 - q_m^2}. \tag{49}$$

For $\phi_e = 1/2$, $q_m/r_0 = 1$, $Pr_0^2 = 0.001$ the resulting r_+ vs τ graph is plotted in Fig. 12. Similar to the canonical ensemble case, below critical pressure, we have three branches of the τ curve in the regions for $\tau < \tau_b$, $\tau_a < \tau < \tau_b$, and $\tau > \tau_a$. The first and third branch are the large black hole and small black hole region and the zero points on these two branches have $w = +1$ and positive specific heat. The other branch represents intermediate black hole region and the zero points in this region have $w = -1$ and negative specific heat. Thus, the topological number is $W = +1 - 1 + 1 = +1$. The generation and annihilation points for $\phi_e = 1/2$, $q_m/r_0 = 1$, $Pr_0^2 = 0.001$ is found at $\tau/r_0 = \tau_a/r_0 = 41.5688$ and $\tau/r_0 = \tau_b/r_0 = 46.9484$ respectively.

Above critical pressure P_c, the same plot is shown in Fig. 13(b). Here, we chose $Pr_0^2 = 0.02$, $q_m = 1$, and $\phi_e = 1/2$. In this case, the unstable region disappears and the $\tau(r_+)$ curve corresponds to stable black hole region. The winding number for each point on the curve is $w = +1$ and the topological number is hence $W = +1$. The unit vector and the zero point for $\tau/r_0 = 35$, $Pr_0^2 = 0.02$, $q_m/r_0 = 1$, and $\phi_e = 1/2$ is shown in Fig. 13(a).

We repeated the exercise altering the values of ϕ_e and q_m/r_0 and observed that the topological number for all the combinations was identical and equal to $W = +1$. The zero points of ϕ^{r_+} is shown in Fig. 14 for $\phi_e = 0.1$, $q_m/r_0 = 0.1$, and $Pr_0^2 = 0.04$.

To understand the impact of the parameter ϕ_e on the thermodynamic topology of the dyonic AdS black hole in the mixed canonical ensemble, we extend our analysis to $\phi_e > 1$ case. In this case, the τ curve has only one black hole branch with winding number $+1$ as shown in Fig. 15. This result is different from the $\phi_e < 1$ case where we have found three branches of the τ curve (see Fig. 12). For any zero point on the τ curve for $\phi_e > 1$ case [Figs. 15(a) and 15(b)], the winding number is $w = +1$ which implies that

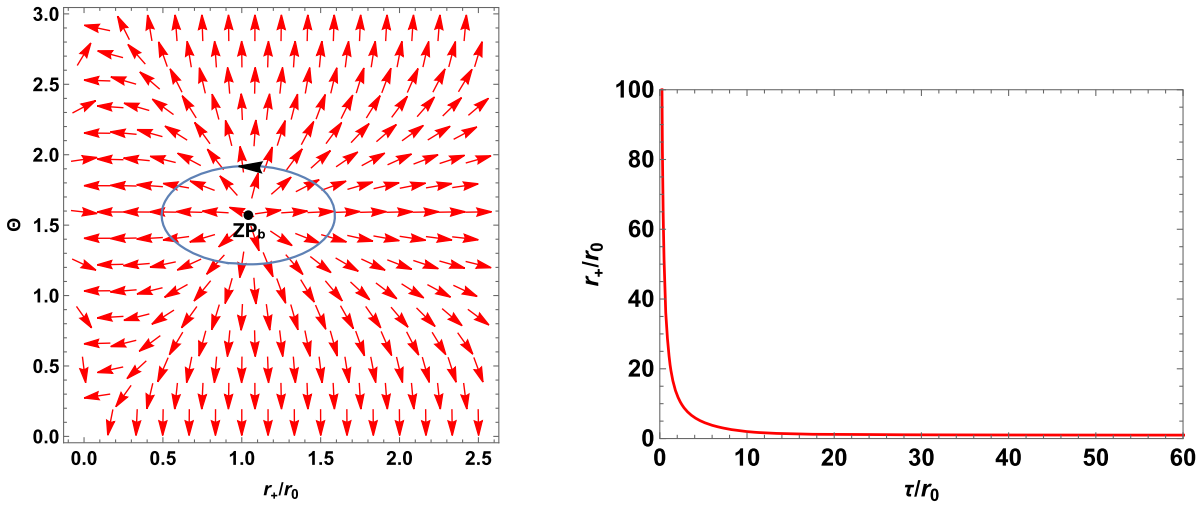

(a) (b)

FIG. 13. Plot of unit vector $n = (n^1, n^2)$ and zero point of ϕ^{r_+} for pressure $Pr_0^2 = 0.02$ (above the critical pressure P_c). (a) Unit vector $n = (n^1, n^2)$ shown in Θ vs r_+/r_0 plane for $Pr_0^2 = 0.02$. The black dot represents zero point. (b) The zero points of ϕ^{r_+} in τ/r_0 vs r_+/r_0 plane for dyonic AdS black hole in mixed ensemble for pressure greater than the critical pressure P_c.

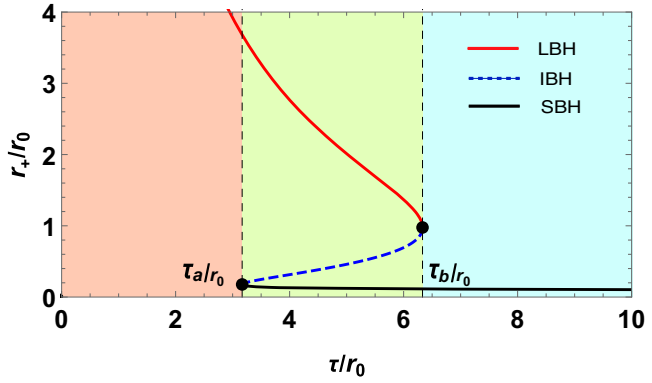

FIG. 14. The zero points of ϕ^{r_+} in τ/r_0 vs r_+/r_0 plane for dyonic AdS black hole in mixed ensemble for $\phi_e = 0.1$, $q_m/r_0 = 0.1$, and $Pr_0^2 = 0.04$.

the topological number is also $W = +1$. This result is similar to that of $\phi_e < 1$ case. Therefore, we conclude that though the critical point as well as the number of black hole branches depends on ϕ_e, they belong to the same topological class.

IV. DYONIC AdS BLACK HOLE IN GRAND CANONICAL ENSEMBLE

In the grand canonical ensemble, both the electric potential ϕ_e and the magnetic potential ϕ_m are kept fixed.

$$\phi_e = \frac{q_e}{r_+}, \quad \text{and} \quad \phi_m = \frac{q_m}{r_+}. \tag{50}$$

The relevant thermodynamic parameters of dyonic AdS black hole in grand canonical ensemble are given by,

$$M = \frac{1}{6} r_+ \{3(\phi_e^2 + \phi_m^2 + 1) + 8\pi P r_+^2\}, \tag{51}$$

$$S = \pi r_+^2, \tag{52}$$

and

$$T = \frac{8\pi P r_+^2 + 1 - \phi_e^2 - \phi_m^2}{4\pi r_+}. \tag{53}$$

A. Topology of dyonic AdS black hole in grand canonical ensemble

Now, we proceed to study the topology of dyonic AdS black hole thermodynamics in grand canonical ensemble. First, we eliminate pressure from (53) using $\left(\frac{\partial_{r_+} T}{\partial_{r_+} S}\right)_{\phi_e,\phi_m,P} = 0$.

$$T = \frac{1 - {\phi_e}^2 - {\phi_m}^2}{2\pi r_+}. \tag{54}$$

The thermodynamics function $\Phi = T/\sin\theta$ is, therefore,

$$\Phi = \frac{\csc\theta(-{\phi_e}^2 - {\phi_m}^2 + 1)}{2\pi r_+}. \tag{55}$$

The components of vector field $\phi = (\phi^{r_+}, \phi^{\theta})$ are

$$\phi^{r_+} = \frac{\csc\theta({\phi_e}^2 + {\phi_m}^2 - 1)}{2\pi r_+^2}, \tag{56}$$

and

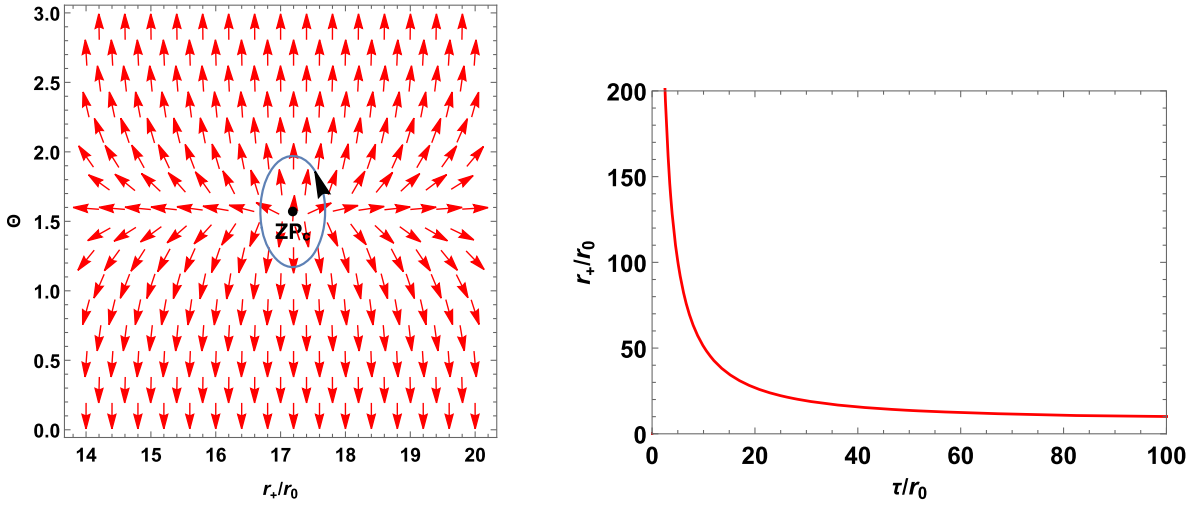

(a) (b)

FIG. 15. Plot of unit vector $n = (n^1, n^2)$ and zero point of ϕ^{r_+} for $\phi_e = 1.5$, $q_m/r_0 = 1$, and $Pr_0^2 = 0.001$. (a) Unit vector $n = (n^1, n^2)$ shown in Θ vs r_+/r_0 plane for $\phi_e > 1$. The black dot represents zero point. (b) The zero points of ϕ^{r_+} in τ/r_0 vs r_+/r_0 plane for $\phi_e > 1$.

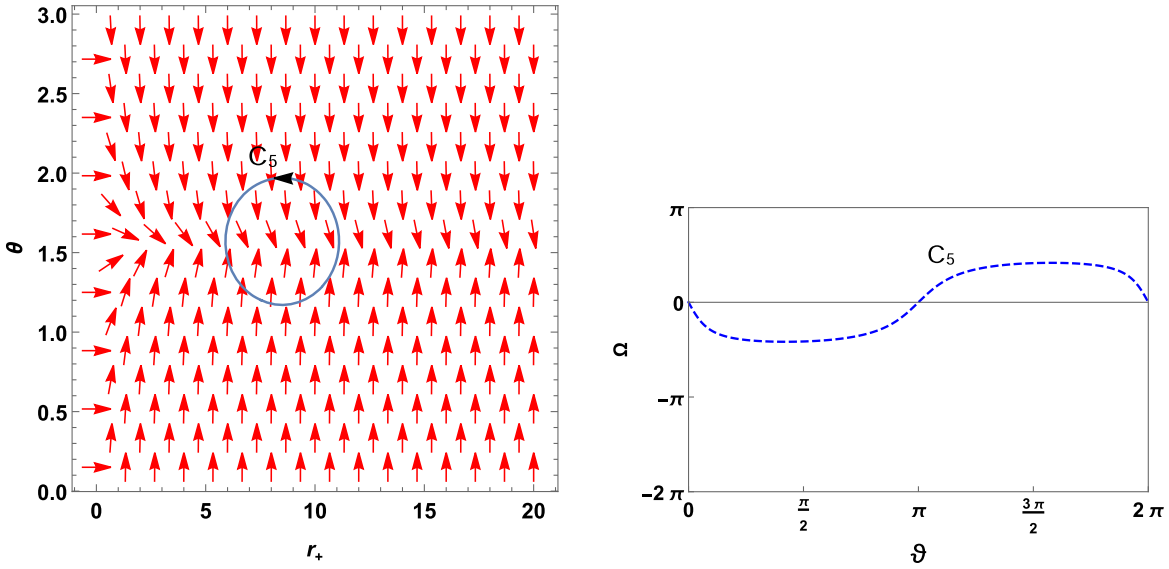

FIG. 16. Plot of vector n in r_+ vs θ plane and the plot of deflection angle $\Omega(\vartheta)$ along C_5. (a) Plot of the normalized vector field n in r_+ vs θ plane for dyonic AdS black hole in grand canonical ensemble. There is no critical point. (b) Ω vs ϑ plot for the contour C_5.

$$\phi^{\theta} = \frac{\cot\theta \csc\theta({\phi_e}^2 + {\phi_m}^2 - 1)}{2\pi r_+}. \tag{57}$$

The normalized vector components are

$$\frac{\phi^{r_+}}{\|\phi\|} = \frac{1}{\sqrt{r_+^2 \cot^2(\theta) + 1}}, \tag{58}$$

and

$$\frac{\phi^{\theta}}{\|\phi\|} = \frac{r_+ \cot(\theta)}{\sqrt{r_+^2 \cot^2(\theta) + 1}}. \tag{59}$$

On following the procedure discussed earlier, we find that this system does not have any critical points [see Fig. 16(a)]. Also, since the contour does not enclose any critical point therefore, the $\Omega(\vartheta)$ function reaches 0 at $\vartheta = 2\pi$ [see Fig. 16(b)].

B. Dyonic AdS black hole solution as topological thermodynamic defects in grand canonical ensemble

Now we identify dyonic AdS black hole as a topological defect in the thermodynamic, and we can use the following general free energy potential:

$$\mathcal{F} = E - \frac{S}{\tau} - q_e\phi_e - q_m\phi_m. \tag{60}$$

Following (8), we calculate the vector components Accordingly, we find the unit vectors

$$\phi^{r_+} = \frac{1}{6}(3\phi_e^2 + 3\phi_m^2 + 8\pi P r_+^2 + 3) - \phi_e^2 - \phi_m^2 + \frac{8}{3}\pi P r_+^2 - \frac{2\pi r_+}{\tau}, \tag{61}$$

and

$$\phi^{\Theta} = -\cot\Theta \csc\Theta. \tag{62}$$

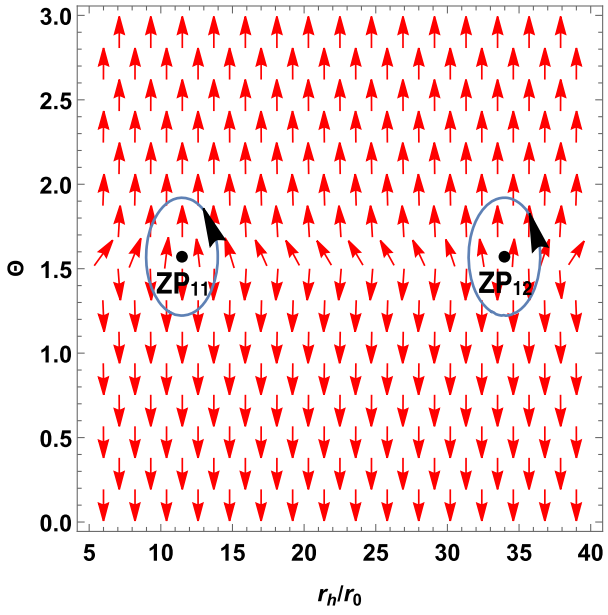

FIG. 17. Unit vector $n = (n^1, n^2)$ shown in Θ vs r_+/r_0 plane for $\tau/r_0 = 110$, $\phi_e = 0.1$, $\phi_m = 0.1$, and $Pr_0^2 = 0.0001$. The black dots represent the zero points.

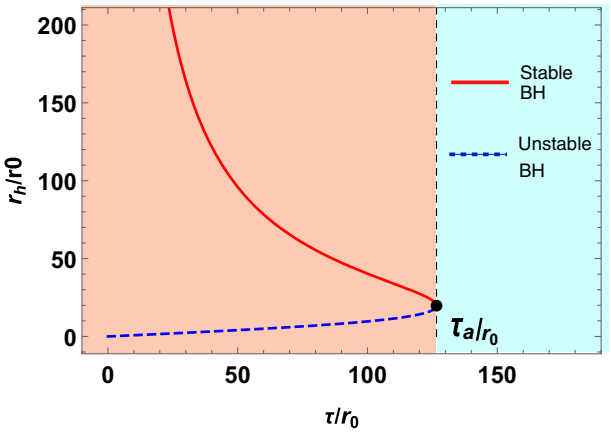

FIG. 18. The zero points of ϕ^{r_+} in τ/r_0 vs r_+/r_0 plane for dyonic AdS black hole in grand canonical ensemble.

For $\tau/r_0 = 110$, $\phi_e = 0.1$, $\phi_m = 0.1$, and $Pr_0^2 = 0.0001$, we find two zero points ZP_{11} and ZP_{12} with winding numbers -1 and $+1$ respectively. These are shown in Fig. 17. Hence, the topological number of dyonic AdS black hole in grand canonical ensemble is 0.

The expression for τ representing zero points is given by

$$\tau = \frac{4\pi r_+}{8\pi P r_+^2 + 1 - \phi_e^2 - \phi_m^2} \tag{63}$$

For $\phi_e = 0.1$, $\phi_m = 0.1$ and $Pr_0^2 = 0.0001$, r_+/r_0 vs τ/r_0 plot is shown in Fig. 18.

In this case, unlike what we saw in canonical and mixed ensembles, the plot exhibits two black hole branches in the regions $\tau < \tau_a$ and $\tau > \tau_a$. The former branch represents unstable black hole region whereas the later branch represents stable black hole region. Any zero point in the unstable and stable region has winding numbers $w = -1$ and $w = +1$ respectively. The topological number is hence $W = 0$ which is different from what we had in canonical and mixed ensembles. The creation point is located at $\tau/r_0 = \tau_a/r_0 = 126.604$.

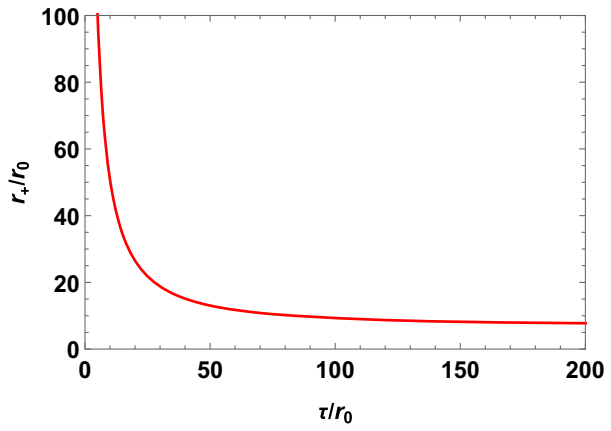

FIG. 19. The zero points of ϕ^{r_+} in τ/r_0 vs r_+/r_0 plane for dyonic AdS black hole in grand canonical ensemble for $\phi_e^2 + \phi_m^2 > 1$ case. Here, we choose $\phi_e = 1$, $\phi_m = 1$, and $Pr_0^2 = 0.001$.

Interestingly, for $\phi_e^2 + \phi_m^2 > 1$, we get only one black hole branch with winding number $+1$ (see Fig. 19). The topological number, therefore, is $+1$. In this case, we do not see any generation or annihilation point.

Thus, in the grand canonical ensemble, for $4d$ dyonic AdS black hole, we have two topological numbers. When $\phi_e^2 + \phi_m^2 < 1$, the topological number is 0 in contrast to what we had in canonical and mixed ensembles. When $\phi_e^2 + \phi_m^2 > 1$, the topological number is 1, same as the ones in canonical and mixed ensembles.

V. CONCLUSION

In this work, we studied the thermodynamic topology of 4d dyonic AdS black hole in canonical, mixed and grand canonical ensembles. Canonical, mixed, and grand canonical ensembles were formed by fixing electric and magnetic charges, magnetic charge, and electric potential and potentials corresponding to both electric and magnetic charges respectively. In all the three ensembles, we evaluated the topological charges of the critical points in their thermodynamic spaces. We observed the presence of a solitary conventional critical point with topological charge -1 in both canonical and mixed ensembles. Contrastingly, in the grand canonical ensemble, no critical point was found. Next, we recognized the dyonic AdS black hole as topological defects in thermodynamic space and analyzed its local and global topology by calculating the winding numbers at the defects. We found that, in both canonical and mixed ensembles, the total topological charge was equal to 1, which was not altered by changes in thermodynamic parameters. In both these ensembles, either one generation and one annihilation points (below critical pressure) or no generation/annihilation points (above critical pressure) were seen. In the grand canonical ensemble, depending on the values of potentials, the total topological charge was found to be either equal to 0 (when $\phi_e^2 + \phi_m^2 < 1$) or 1 (when $\phi_e^2 + \phi_m^2 > 1$). In this ensemble, we found either one generation point (when $\phi_e^2 + \phi_m^2 < 1$) or no generation/annihilation point (when $\phi_e^2 + \phi_m^2 > 1$).

From our analysis, we conclude that 4d dyonic AdS black hole in canonical and mixed ensembles can be placed in the same thermodynamic topological class. However, the thermodynamic topology of 4d dyonic AdS black hole in grand canonical ensemble is different from those in the other two ensembles. Or in other words, the topological class of 4d dyonic AdS black hole is ensemble dependent. It will be interesting to extend the study of ensemble dependent thermodynamic topology to other black holes with rich phase structures. We plan to do so in our future works.

[1] S. W. Hawking, Black hole explosions?, Nature (London) **248**, 30 (1974).
[2] J. D. Bekenstein, Black holes and entropy, Phys. Rev. D **7**, 2333 (1973).
[3] S. W. Hawking, Particle creation by black holes, Commun. Math. Phys. **43**, 199 (1975); **46**, 206(E) (1976).
[4] J. D. Bekenstein, Black holes and the second law, Lett. Nuovo Cimento **4**, 737 (1972).
[5] James M. Bardeen, B. Carter, and S. W. Hawking, The four laws of black hole mechanics, Commun. Math. Phys. **31**, 161 (1973).
[6] Robert M. Wald, Entropy and black-hole thermodynamics, Phys. Rev. D **20**, 1271 (1979).
[7] Jacob D. Bekenstein, Black-hole thermodynamics, Phys. Today **33**, No. 1, 24 (1980).
[8] R. M. Wald, The thermodynamics of black holes, Living Rev. Relativity **4**, 6 (2001).
[9] S. Carlip, Black hole thermodynamics, Int. J. Mod. Phys. D **23**, 1430023 (2014).
[10] A. C. Wall, A survey of black hole thermodynamics, arXiv:1804.10610.
[11] P. Candelas and D. W. Sciama, Irreversible Thermodynamics of Black Holes, Phys. Rev. Lett. **38**, 1372 (1977).
[12] A. Chamblin, R. Emparan, C. V. Johnson, and R. C. Myers, Holography, thermodynamics and fluctuations of charged AdS black holes, Phys. Rev. D **60**, 104026 (1999).
[13] S. W. Hawking and D. N. Page, Thermodynamics of black holes in anti-de Sitter space, Commun. Math. Phys. **87**, 577 (1983).
[14] A. Chamblin, R. Emparan, C. V. Johnson, and R. C. Myers, Charged AdS black holes and catastrophic holography, Phys. Rev. D **60**, 064018 (1999).
[15] D. Kubiznak and R. B. Mann, P-V criticality of charged AdS black holes, J. High Energy Phys. 07 (2012) 033.
[16] N. Altamirano, D. Kubiznak, and R. B. Mann, Reentrant phase transitions in rotating anti–de Sitter black holes, Phys. Rev. D **88**, 101502 (2013).
[17] N. Altamirano, D. Kubizňák, R. B. Mann, and Z. Sherkatghanad, Kerr-AdS analogue of triple point and solid/liquid/gas phase transition, Classical Quantum Gravity 2014) 042001 ,**31**).
[18] S. W. Wei and Y. X. Liu, Triple points and phase diagrams in the extended phase space of charged Gauss-Bonnet black holes in AdS space, Phys. Rev. D **90**, 044057 (2014).
[19] A. M. Frassino, D. Kubiznak, R. B. Mann, and F. Simovic, Multiple reentrant phase transitions and triple points in Lovelock thermodynamics, J. High Energy Phys. 09 (2014) 080.
[20] R. G. Cai, L. M. Cao, L. Li, and R. Q. Yang, P-V criticality in the extended phase space of Gauss-Bonnet black holes in AdS space, J. High Energy Phys. 09 (2013) 005.
[21] H. Xu, W. Xu, and L. Zhao, Extended phase space thermodynamics for third order Lovelock black holes in diverse dimensions, Eur. Phys. J. C **74**, 3074 (2014).
[22] B. P. Dolan, A. Kostouki, D. Kubiznak, and R. B. Mann, Isolated critical point from Lovelock gravity, Classical Quantum Gravity **31**, 242001 (2014).
[23] R. A. Hennigar, W. G. Brenna, and R. B. Mann, P-V criticality in quasitopological gravity, J. High Energy Phys. 07 (2015) 077.
[24] R. A. Hennigar and R. B. Mann, Reentrant phase transitions and van der Waals behaviour for hairy black holes, Entropy **17**, 8056 (2015).
[25] R. A. Hennigar, R. B. Mann, and E. Tjoa, Superfluid Black Holes, Phys. Rev. Lett. **118**, 021301 (2017).
[26] D. C. Zou, R. Yue, and M. Zhang, Reentrant phase transitions of higher-dimensional AdS black holes in dRGT massive gravity, Eur. Phys. J. C **77**, 256 (2017).
[27] D. Kastor, S. Ray, and J. Traschen, Enthalpy and the mechanics of AdS black holes, Classical Quantum Gravity **26**, 195011 (2009).
[28] S. Gunasekaran, R. B. Mann, and D. Kubiznak, Extended phase space thermodynamics for charged and rotating black holes and Born-Infeld vacuum polarization, J. High Energy Phys. 11 (2012) 110.
[29] B. P. Dolan, Where is the PdV in the first law of black hole thermodynamics?, arXiv:1209.1272.
[30] D. Chen, G. qingyu, and J. Tao, The modified first laws of thermodynamics of anti-de Sitter and de Sitter space-times, Nucl. Phys. **B918**, 115 (2017).
[31] S. W. Wei and Y. X. Liu, Topology of black hole thermodynamics, Phys. Rev. D **105**, 104003 (2022).
[32] Y. S. Duan, The structure of the topological current, Report No. SLAC-PUB-3301, 1984.
[33] Y. S. Duan and M. L. Ge, SU(2) gauge theory and electrodynamics with N magnetic monopoles, Sci. Sin. **9**, 1072 (1979).
[34] P. K. Yerra and C. Bhamidipati, Topology of black hole thermodynamics in Gauss-Bonnet gravity, Phys. Rev. D **105**, 104053 (2022).
[35] N. C. Bai, L. Li, and J. Tao, Topology of black hole thermodynamics in Lovelock gravity, Phys. Rev. D **107**, 064015 (2023).
[36] P. K. Yerra and C. Bhamidipati, Topology of Born-Infeld AdS black holes in 4D novel Einstein-Gauss-Bonnet gravity, Phys. Lett. B **835**, 137591 (2022).
[37] S. W. Wei and Y. X. Liu, Topology of equatorial timelike circular orbits around stationary black holes, Phys. Rev. D **107**, 064006 (2023).
[38] P. K. Yerra, C. Bhamidipati, and S. Mukherji, Topology of critical points and Hawking-Page transition, Phys. Rev. D **106**, 064059 (2022).
[39] M. B. Ahmed, D. Kubiznak, and R. B. Mann, Vortex-antivortex pair creation in black hole thermodynamics, Phys. Rev. D **107**, 046013 (2023).
[40] N. C. Bai, L. Song, and J. Tao, Reentrant phase transition in holographic thermodynamics of Born-Infeld AdS black hole, arXiv:2212.04341.
[41] S. W. Wei, Y. X. Liu, and R. B. Mann, Black Hole Solutions as Topological Thermodynamic Defects, Phys. Rev. Lett. **129**, 191101 (2022).
[42] D. Wu, Topological classes of rotating black holes, Phys. Rev. D **107**, 024024 (2023).
[43] C. Liu and J. Wang, Topological natures of the Gauss-Bonnet black hole in AdS space, Phys. Rev. D **107**, 064023 (2023).
[44] Z. Y. Fan, Topological interpretation for phase transitions of black holes, Phys. Rev. D **107**, 044026 (2023).
[45] C. Fang, J. Jiang, and M. Zhang, Revisiting thermodynamic topologies of black holes, J. High Energy Phys. 01 (2023) 102.

[46] X. Ye and S. W. Wei, Topological study of equatorial timelike circular orbit for spherically symmetric (hairy) black holes, J. Cosmol. Astropart. Phys. 07 (2023) 049.
[47] M. Zhang and J. Jiang, Bulk-boundary thermodynamic equivalence: A topology viewpoint, J. High Energy Phys. 06 (2023) 115.
[48] Y. Du and X. Zhang, Topological classes of black holes in de-Sitter spacetime, arXiv:2303.13105.
[49] T. Sharqui, Topological nature of black hole solutions in massive gravity, arXiv:2304.02889.
[50] Y. Du and X. Zhang, Topological classes of BTZ black holes, arXiv:2302.11189.
[51] D. Wu and S. Q. Wu, Topological classes of thermodynamics of rotating AdS black holes, Phys. Rev. D **107**, 084002 (2023).
[52] D. Wu, Classifying topology of consistent thermodynamics of the four-dimensional neutral Lorentzian NUT-charged spacetimes, Eur. Phys. J. C **83**, 365 (2023).
[53] P. Dobiasch and D. Maison, Stationary, spherically symmetric solutions of Jordan's unified theory of gravity and electromagnetism, Gen. Relativ. Gravit. **14**, 231 (1982).
[54] G. W. Gibbons and R. E. Kallosh, Topology, entropy and Witten index of dilaton black holes, Phys. Rev. D **51**, 2839 (1995).
[55] D. Rasheed, The rotating dyonic black holes of Kaluza-Klein theory, Nucl. Phys. **B454**, 379 (1995).
[56] B. A. Campbell, N. Kaloper, R. Madden, and K. A. Olive, Physical properties of four-dimensional superstring gravity black hole solutions, Nucl. Phys. **B399**, 137 (1993).
[57] G. J. Cheng, R. R. Hsu, and W. F. Lin, Dyonic black holes in string theory, J. Math. Phys. (N.Y.) **35**, 4839 (1994).
[58] H. Lü, Y. Pang, and C. N. Pope, AdS dyonic black hole and its thermodynamics, J. High Energy Phys. 11 (2013) 033.
[59] S. Dutta, A. Jain, and R. Soni, Dyonic black hole and holography, J. High Energy Phys. 12 (2013) 060.